INTERNATIONAL JOURNAL FOR NUMERICAL METHODS IN FLUIDS, VOL. 9, 1517–1537 (1989)

HIGH-ORDER AXISYMMETRIC NAVIER–STOKES CODE: DESCRIPTION AND EVALUATION OF BOUNDARY CONDITIONS

J. N. SØRENSEN

Department of Fluid Mechanics, Technical University of Denmark, DK-2800 Lyngby, Denmark

AND

TA PHUOC LOC

LIMSI/CNRS, F-91406 Orsay Cedex, France and ONERA, F-92322 Châtillon Cedex, France

SUMMARY

A description is given of a high-order solution algorithm for the solution of the unsteady axisymmetric Navier–Stokes equations. The method consists of a combination of fourth-order and second-order accurate finite difference schemes, where the approximated equations are solved by an alternating direction implicit (ADI) method. Special attention is paid to the boundary conditions. Results are compared with measurements for the cases of rotating flow within a closed cylinder (rotating driven cavity), developing axial flow in a stationary pipe and developing flow in a rotating pipe.

KEY WORDS Navier–Stokes equations Boundary conditions Higher order finite difference method

1. INTRODUCTION

The simulation of rotating fluid flows has many important applications in nature as well as in industrial environments. To obtain a closer understanding of the various fluid dynamical processes underlying rotating flows, we present here an accurate numerical method aimed at the study of transitional and turbulent flows by direct simulations of the unsteady, axisymmetric Navier–Stokes equations.

The method which has been developed at Laboratoire d'Informatique pour la Mecanique et les Sciences de l'Ingenieur (LIMSI) has in various cases been shown to accurately predict two-dimensional flows (see e.g. References 1–3).

The extension of the method to axisymmetric flows is based on a ψ–ω–Γ (streamfunction–vorticity–circulation) formulation and, as in the two-dimensional case, takes advantage of a combination of finite difference schemes of order $o(h^4)$ and $o(h^2)$ solved by an efficient ADI algorithm.

Owing to the high accuracy of the method, special attention is paid to the formulation of stable boundary conditions.

In the present work results will be shown for the following cases:

(1) rotating flow in a cylindrical vessel initiated by a rotating cover (rotating cavity flow)

0271–2091/89/121517–21$10.50 *Received November 1988*

(2) developing, non-rotating flow in a stationary pipe
(3) developing flow in a rotating pipe.

Whenever possible, the results obtained will be compared with experimental observations.

2. FORMULATION OF THE GOVERNING EQUATIONS

Assuming axial symmetry and incompressible flow conditions, in terms of cylindrical coordinates (r^*, θ^*, z^*) with corresponding velocity components (u^*, v^*, w^*) the momentum equations and the equation of continuity may be written as

$$\frac{\partial u^*}{\partial t^*}+u^*\frac{\partial u^*}{\partial r^*}+w^*\frac{\partial u^*}{\partial z^*}-\frac{v^{*2}}{r^*}=-\frac{1}{\rho}\frac{\partial p^*}{\partial r^*}+\nu\left(\frac{\partial^2 u^*}{\partial r^{*2}}+\frac{1}{r^*}\frac{\partial u^*}{\partial r^*}+\frac{\partial^2 u^*}{\partial z^{*2}}-\frac{u^*}{r^{*2}}\right), \tag{1}$$

$$\frac{\partial v^*}{\partial t^*}+u^*\frac{\partial v^*}{\partial r^*}+w^*\frac{\partial v^*}{\partial z^*}+\frac{u^*v^*}{r^*}=\nu\left(\frac{\partial^2 v^*}{\partial r^{*2}}+\frac{1}{r^*}\frac{\partial v^*}{\partial r^*}+\frac{\partial^2 v^*}{\partial z^{*2}}-\frac{v^*}{r^{*2}}\right), \tag{2}$$

$$\frac{\partial w^*}{\partial t^*}+u^*\frac{\partial w^*}{\partial r^*}+w^*\frac{\partial w^*}{\partial z^*}=-\frac{1}{\rho}\frac{\partial p^*}{\partial z^*}+\nu\left(\frac{\partial^2 w^*}{\partial r^{*2}}+\frac{1}{r^*}\frac{\partial w^*}{\partial r^*}+\frac{\partial^2 w^*}{\partial z^{*2}}\right), \tag{3}$$

$$\frac{\partial(u^*r^*)}{\partial r^*}+\frac{\partial(w^*r^*)}{\partial z^*}=0, \tag{4}$$

where p^* denotes the pressure, t^* the time variable, ν the kinematic viscosity and ρ the fluid density. Furthermore, we introduce a local circulation Γ^* and in the r^*-z^* plane a streamfunction ψ^* and a vorticity ω^* as follows:

$$\Gamma^*=r^*v^*, \tag{5}$$

$$\partial\psi^*/\partial z^*=r^*u^*, \tag{6}$$

$$\partial\psi^*/\partial r^*=-r^*w^*, \tag{7}$$

$$\omega^*=\partial u^*/\partial z^*-\partial w^*/\partial r^*. \tag{8}$$

Introducing a characteristic length δ^* and a characteristic velocity $\bar{w}^*$, the variables are made dimensionless as

$$\begin{aligned} &r=r^*/\delta^*, && z=z^*/\delta^*, && t=t^*\bar{w}^*/\delta^*,\\ &u=u^*/\bar{w}^*, && v=v^*/\bar{w}^*, && w=w^*/\bar{w}^*,\\ &\psi=\psi^*/\bar{w}^*\delta^{*2}, && \omega=\omega^*\delta^*/\bar{w}^*, && \Gamma=\Gamma^*/\delta^*\bar{w}^*. \end{aligned} \tag{9}$$

In order to stretch the net and eventually extend it to infinity in the r-direction, we introduce a transformation as

$$y=y(r) \tag{10}$$

Comparing equations (1)–(10) and formally replacing z by x, the governing equations are now written as

$$u=\frac{1}{r}\frac{\partial\psi}{\partial x}, \tag{11}$$

$$w=-\frac{f}{r}\frac{\partial\psi}{\partial y}, \tag{12}$$

$$\omega r = \frac{\partial^2 \psi}{\partial x^2} + \left(g - \frac{f}{r}\right)\frac{\partial \psi}{\partial y} + f^2 \frac{\partial^2 \psi}{\partial y^2}, \tag{13}$$

$$Re\left(\frac{\partial \Gamma}{\partial t} + \frac{\partial (w\Gamma)}{\partial x} + f\frac{\partial (u\Gamma)}{\partial y} + \frac{u\Gamma}{r}\right) = \frac{\partial^2 \Gamma}{\partial x^2} + \left(g - \frac{f}{r}\right)\frac{\partial \Gamma}{\partial y} + f^2 \frac{\partial^2 \Gamma}{\partial y^2}, \tag{14}$$

$$Re\left[\frac{\partial \omega}{\partial t} + \frac{\partial (w\omega)}{\partial x} + f\frac{\partial (u\omega)}{\partial y} - \frac{\partial}{\partial x}\left(\frac{\Gamma^2}{r^3}\right)\right] = \frac{\partial^2 \omega}{\partial x^2} + \left(g + \frac{f}{r}\right)\frac{\partial \omega}{\partial y} + f^2 \frac{\partial^2 \omega}{\partial y^2} - \frac{\omega}{r^2}, \tag{15}$$

where

$$f = \partial y / \partial r, \tag{16}$$

$$g = \partial^2 y / \partial r^2, \tag{17}$$

$$Re = \bar{w}^* \delta^* / \nu. \tag{18}$$

3. NUMERICAL METHOD

The transformed Navier–Stokes equations defined by (11)–(15) consist of two definition equations for the velocities u and w, a Poisson equation for the streamfunction ψ, a momentum equation for the circulation Γ and a momentum equation for the velocity ω. The solution of these equations is accomplished by employing a finite difference approximation in combination with an alternating direction implicit (ADI) technique,[4] where a fourth-order accurate discretization is utilized for the solution of the velocities and the streamfunction, and a second-order accurate one is utilized for the circulation and the vorticity. The time derivatives are everywhere discretized by first-order accurate formulae.

3.1. Solution procedure of the Poisson equation

To solve the ψ-equation with fourth-order accuracy, a compact formulation based on three-point Hermitian-formulae is employed. The formulae take the form (see e.g. Reference 5 or 6)

$$F'_{i+1} + 4F'_i + F'_{i-1} = \frac{3}{h}(F_{i+1} - F_{i-1}) + o(h^4), \tag{19}$$

$$F''_{i+1} + 10F''_i + F''_{i-1} = \frac{12}{h^2}(F_{i+1} - 2F_i + F_{i-1}) + o(h^4), \tag{20}$$

where h denotes the mesh size, subscript 'i' refers to the point being calculated, and $(\,)'$ and $(\,)''$ denote first derivative and second derivative respectively.

Solving equations (19) and (20) in combination with the governing equation for the variable F (in our case ψ of equation (13)) assures fourth-order accuracy at the expense of two additional variables F' and F'' being introduced. The advantage of this method is that, for a given accuracy, the fourth-order scheme makes it possible to diminish the number of grid points in comparison with methods of lower order. The expense, however, is that two additional equations with two additional variables have to be solved. In our case equations (19) and (20) are solved together with the equations for u, w and ψ, equations (11)–(13).

To optimize the solution procedure, an ADI algorithm of the Peaceman–Rachford type is utilized when solving equation (13). As shown by Wachpress,[7] this algorithm is most effectively employed when going through 2^N iterations at each time step, where N in our case takes the value 2 or 3.

Letting the first semi-step at the local iteration step k be in the y-direction, the resulting system of equations reads

$$\lambda_k \psi_{i,j}^{n,k+1/2} - \left(g - \frac{f}{r}\right)_j \left(\frac{\partial \psi}{\partial y}\right)_{i,j}^{n,k+1/2} - f_j^2 \left(\frac{\partial^2 \psi}{\partial y^2}\right)_{i,j}^{n,k+1/2} = -\omega_{i,j}^n r_j + \lambda_k \psi_{i,j}^{n,k} + \left(\frac{\partial^2 \psi}{\partial x^2}\right)_{i,j}^{n,k}, \tag{21}$$

$$\left(\frac{\partial \psi}{\partial y}\right)_{i,j+1}^{n,k+1/2} + 4\left(\frac{\partial \psi}{\partial y}\right)_{i,j}^{n,k+1/2} + \left(\frac{\partial \psi}{\partial y}\right)_{i,j-1}^{n,k+1/2} = \frac{3}{(\Delta y)^2}(\psi_{i,j+1}^{n,k+1/2} - \psi_{i,j-1}^{n,k+1/2}), \tag{22}$$

$$\left(\frac{\partial^2 \psi}{\partial y^2}\right)_{i,j+1}^{n,k+1/2} + 10\left(\frac{\partial^2 \psi}{\partial y^2}\right)_{i,j}^{n,k+1/2} + \left(\frac{\partial^2 \psi}{\partial y^2}\right)_{i,j-1}^{n,k+1/2} = \frac{12}{(\Delta y)^2}(\psi_{i,j+1}^{n,k+1/2} - 2\psi_{i,j}^{n,k+1/2} + \psi_{i,j-1}^{n,k+1/2}), \tag{23}$$

where λ_k is introduced in order to optimize the convergence.[7] Here superscript 'n' denotes the time step and the discretization in the x- and y-direction is given by the subscripts $i = 1, 2, \ldots, NX$ and $j = 1, 2, \ldots, NY$ respectively.

The unknown $(\partial^2 \psi / \partial y^2)_{i,j}^{n,k+1/2}$ is eliminated by combining equations (21) and (23), and the solution of $\psi_{i,j}^{n,k+1/2}$ and $(\partial \psi / \partial y)_{i,j}^{n,k+1/2}$ is accomplished by solving the resulting 2×2 block-tridiagonal system of equations by a factorization method. The solution of the second semi-step is accomplished in a similar way by taking the derivatives in the x-direction as unknowns and solving equation (13) in combination with equation (23) for $\psi_{i,j}^{n,k+1}$. As a result of the solution procedure, the derivatives of ψ are determined directly; therefore the velocities are calculated straightforwardly from the definition equations (11) and (12).

3.2. *Solution procedure of the momentum equations*

To calculate ω and Γ of equations (14) and (15), a two-step Peaceman–Rachford[4] algorithm is utilized in combination with a second-order finite difference scheme. In some cases it may be convenient to reduce the accuracy to obtain stable solutions. This is accomplished here by using an alternating 'plus/minus' upwind discretization of the convective terms, thus assuring diagonal dominance without destroying the accuracy too much. Letting the first semi-step be in the y-direction, the Γ-equation is written as

$$Re\left(\frac{\Gamma_{i,j}^{n+1/2} - \Gamma_{i,j}^n}{\Delta t/2} + f_j[\alpha_{ij}\delta_y^- + (1-\alpha_{ij})\delta_y^+](u_{i,j}^n \Gamma_{i,j}^{n+1/2}) + \alpha_{ij}\frac{u_{i,j}^n \Gamma_{i,j}^{n+1/2}}{r_j}\right)$$
$$- f_j^2 \delta_{yy}^2 \Gamma_{i,j}^{n+1/2} - \left(g - \frac{f}{r}\right)_j \delta_y \Gamma_{i,j}^{n+1/2}$$
$$= -Re\left([(1-\beta_{ij})\delta_x^- + \beta_{ij}\delta_x^+](w_{i,j}^n \Gamma_{i,j}^n) + (1-\alpha_{ij})\frac{u_{i,j}^n \Gamma_{i,j}^n}{r_j}\right) + \delta_{xx}^2 \Gamma_{i,j}^n, \tag{24}$$

where Δt defines the explicit time step.

Putting $\alpha_{ij} = 1/2$ and $\beta_{ij} = 1/2$ defines central differences, and letting

$$\alpha_{ij} = \begin{cases} 1 & \text{for } u_{i,j}^n \geqslant 0 \\ 0 & \text{for } u_{i,j}^n < 0 \end{cases} \qquad \text{and} \qquad \beta_{ij} = \begin{cases} 1 & \text{for } w_{i,j}^n \geqslant 0 \\ 0 & \text{for } w_{i,j}^n < 0 \end{cases}$$

determines the upwind discretization.

The upwinding parameters are defined as

$$\delta_y^+(\,)_{i,j} = [(\,)_{i,j+1} - (\,)_{i,j}]/\Delta y,$$
$$\delta_y^-(\,)_{i,j} = [(\,)_{i,j} - (\,)_{i,j-1}]/\Delta y,$$

and δ_y and δ_{yy} denote the usual central difference operators.

Correcting the upwinded terms by the alternating discretization, the second semi-step in the x-direction is written as

$$Re\left(\frac{\Gamma_{i,j}^{n+1}-\Gamma_{i,j}^{n+1/2}}{\Delta t/2}+[\beta_{ij}\delta_x^- +(1-\beta_{ij})\delta_x^+](w_{i,j}^n\Gamma_{i,j}^{n+1})+\alpha_{ij}\frac{u_{i,j}^n\Gamma_{i,j}^{n+1}}{r_j}\right)-\delta_{xx}^2\Gamma_{i,j}^{n+1}$$
$$=-Re\left(f_j[(1-\alpha_{ij})\delta_y^- +\alpha_{ij}\delta_y^+](u_{i,j}^n\Gamma_{i,j}^{n+1/2})+(1-\alpha_{ij})\frac{u_{i,j}^n\Gamma_{i,j}^{n+1/2}}{r_j}\right)+\left(g-\frac{f}{r}\right)_j\delta_y\Gamma_{i,j}^{n+1/2}$$
$$+f_j^2\delta_{yy}\Gamma_{i,j}^{n+1/2}. \tag{25}$$

A similar procedure is employed when solving equation (15) for the vorticity ω.

4. TEST CASES AND EVALUATION OF BOUNDARY CONDITIONS

The high-order scheme introduced in the previous section is unconditionally stable. To maintain this property it is essential to derive a set of stable boundary conditions which do not destroy the order of the overall flow problem. In this section a number of different boundary conditions will be tested on some selected flow problems.

Common to all the cases treated is the symmetry condition along the line $y=0$. Denoting points located on this line by $j=1$ and neighbouring points by $j=2$ inside the flow domain and $j=-2$ outside the flow domain, the symmetry conditions may be written as

$$u_{i,1}=\Gamma_{i,1}=\omega_{i,1}=0, \tag{26a}$$

$$\psi_{i,1}=\left(\frac{\partial\psi}{\partial y}\right)_{i,1}=0, \tag{26b}$$

$$\left(\frac{\partial^{(n)}\psi}{\partial y^{(n)}}\right)_{i,-2}=(-1)^n\left(\frac{\partial^{(n)}\psi}{\partial y^{(n)}}\right)_{i,2}, \tag{26c}$$

where equation (26c) reflects the fact that $\psi(y)$ is an even function about the symmetry line.

Evaluating the Hermitian formulae (19) and (20), it is easily seen that equation (19) is identically satisfied whereas equation (20) yields the relation

$$\left(\frac{\partial^2\psi}{\partial y^2}\right)_{i,1}=\frac{2{\cdot}4}{(\Delta y)^2}\psi_{i,2}-0{\cdot}2\left(\frac{\partial^2\psi}{\partial y^2}\right)_{i,2}+o[(\Delta y)^4]. \tag{27}$$

Substituting equation (27) into the Hermitian formulae as $j=2$, the resulting fourth-order accurate boundary condition may be written as

$$\left(\frac{\partial^2\psi}{\partial y^2}\right)_{i,3}+9{\cdot}8\left(\frac{\partial^2\psi}{\partial y^2}\right)_{i,2}=\frac{12}{(\Delta y)^2}(\psi_{i,3}-2{\cdot}2\psi_{i,2})+o[(\Delta y)^4]. \tag{28}$$

When solving the Poisson equation along a line $x=$ constant, this equation replaces equation (23) at the first point after the symmetry line. The axial velocity may be found from the definition equation (12):

$$w_{i,1}=-f_{i,1}^2\left(\frac{\partial^2\psi}{\partial y^2}\right)_{i,1}. \tag{29}$$

4.1. Rotating flow in a closed circular cylinder

To study the behaviour under no-slip conditions, we analyse here the influence of the boundary conditions on the solution of a rotating flow in a closed cylindrical container with a circular cross-section. The circulation of the flow is created by letting the cover rotate, as shown in Figure 1.

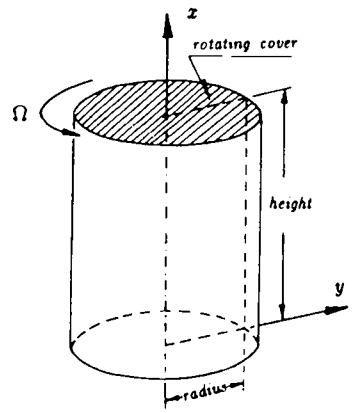

Figure 1. Geometry of the cylinder

This case is particularly interesting because of its simple geometry and because it may exhibit a large variety of different flow structures, depending on the aspect ratio (height to radius) and Reynolds number. For example, at the centreline, axial stagnation points and separation bubbles, which can be interpreted as vortex breakdown, may occur.

The configuration has been the subject of many experimental and numerical investigations. Escudier[8] made some visualizations of flow structures at different aspect ratios and Reynolds numbers and showed that up to three isolated recirculating bubbles may be created at the symmetry line. Michelsen[9] made detailed LDA measurements of the velocity distribution in a container with aspect ratio 1·0 and Reynolds number 1800 in order to test his axisymmetric finite element code.

Denoting the height of the cylinder as H, the radius as R and letting it rotate with rotational speed Ω, the variables are made dimensionless by introducing the characteristic quantities

$$\bar{w}^* = \Omega R, \qquad \delta^* = R.$$

Thus the Reynolds number is given as $Re = \Omega R^2/\nu$, and $x \in [0, H/R]$ and $y \in [0, 1]$.

At all boundaries we have no-slip conditions:

$$x = 0: \quad u = w = \psi = \partial\psi/\partial x = 0, \quad \Gamma = r^2, \tag{30a}$$

$$x = H/R: u = w = \psi = \partial\psi/\partial x = \Gamma = 0, \tag{30b}$$

$$y = 1: \quad u = w = \psi = \partial\psi/\partial y = \Gamma = 0. \tag{30c}$$

To determine the conditions for the vorticity and the second derivatives of the streamfunction, we employ the relations

$$\omega r = \partial^2\psi/\partial x^2 \qquad \text{at } x = \text{constant boundaries}, \tag{31}$$

$$\omega r = f^2(\partial^2\psi/\partial y^2) \quad \text{at } y = \text{constant boundaries}, \tag{32}$$

and perform a Taylor expansion from the boundary considered into the flow domain. Taking for example the boundary $x = 0$, we get

$$\psi_{2,j} = \psi_{1,j} + \Delta x \left(\frac{\partial\psi}{\partial x}\right)_{1,j} + \frac{(\Delta x)^2}{2}\left(\frac{\partial^2\psi}{\partial x^2}\right)_{1,j} + \frac{(\Delta x)^3}{6}\left(\frac{\partial^3\psi}{\partial x^3}\right)_{1,j} + o[(\Delta x)^4]. \tag{33}$$

Neglecting the third-order derivative, a first-order boundary condition for the second-order derivative of the streamfunction may be established as follows:

$$\left(\frac{\partial^2\psi}{\partial x^2}\right)_{1,j}=\frac{2}{(\Delta x)^2}(\psi_{2,j}-\psi_{1,j})-\frac{2}{\Delta x}\left(\frac{\partial\psi}{\partial x}\right)_{1,j}+o(\Delta x). \tag{34}$$

In order to obtain a second-order boundary condition, we make an additional Taylor expansion

$$\psi_{3,j}=\psi_{1,j}+2\Delta x\left(\frac{\partial\psi}{\partial x}\right)_{1,j}+\frac{(2\Delta x)^2}{2}\left(\frac{\partial^2\psi}{\partial x^2}\right)_{1,j}+\frac{(2\Delta x)^3}{6}\left(\frac{\partial^3\psi}{\partial x^3}\right)_{1,j}+o[(\Delta x)^4]. \tag{35}$$

Multiplying equation (33) by 8 and subtracting it from equation (35) eliminates the third-order derivative to give the general formula

$$\left(\frac{\partial^2\psi}{\partial x^2}\right)_{1,j}=\frac{1}{2(\Delta x)^2}(-7\psi_{1,j}+8\psi_{2,j}-\psi_{3,j})-\frac{3}{\Delta x}\left(\frac{\partial\psi}{\partial x}\right)_{1,j}+o[(\Delta x)^2]. \tag{36}$$

Equations (34) and (36) define Dirichlet conditions for both the Poisson equation and, employing the relation (31), the vorticity momentum equation.

The last boundary condition to be tested is a second-order accurate one for the vorticity, which is obtained by approximating the third-order derivative of equation (33) by a two-point, one-sided discretization. Replacing second-order derivatives of the streamfunction by ω, according to equation (31), we get

$$2\omega_{1,j}+\omega_{2,j}=\left[\frac{6}{(\Delta x)^2}(\psi_{1,j}+\psi_{2,j})-\frac{6}{\Delta x}\left(\frac{\partial\psi}{\partial x}\right)_{1,j}\right]\Big/r_j+o[(\Delta x)^2]. \tag{37}$$

Thus we have here a Neumann condition for the vorticity which is employed directly in the momentum equation. The second-order derivative of the streamfunction is found from equation (31).

The first case to be calculated consists of a cylinder with aspect ratio $H/R=2$ and Reynolds number $Re=1854$. This particular case has been chosen because it corresponds to one of the flow cases visualized by Escudier[8] and has recently been calculated by Lugt and Abboud.[10]

To determine the number of grid points necessary to obtain grid-independent solutions, a series of calculations with different space discretization have been performed. The outcome of this study is shown in Figure 2, where the axial velocity distribution along the symmetry line is shown for different grid sizes. Note here that the main flow along the symmetry line is in the opposite direction to the coordinate axis; hence positive velocities define recirculating flow conditions. It is seen here that all the solutions except the coarsest (51×51) case show the same trends, and it was found that in order to obtain solutions within acceptable accuracy, a discretization of 91×71 was sufficient. In the following a discretization of 101×71 grid points will be employed.

The influence of the boundary conditions is shown in Figure 3, where time histories of the axial velocity component of a point located at the symmetry line at approximately $x=0{\cdot}8$ have been compared for different boundary conditions. It is seen here that the two second-order accurate boundary conditions give time histories which are in close agreement with each other, whereas the history of the first-order condition exhibits a delaying effect in time and ends with a stationary value which is different from the other two. It is likely here that this difference can be attributed to the closed, wall-driven configuration of the flow domain. Thus if any error or perturbation is imposed on one of the boundaries, it will, owing to the convection along the walls, be transported to all the other boundaries, including the boundary defining the axis of symmetry, in the calculation domain.

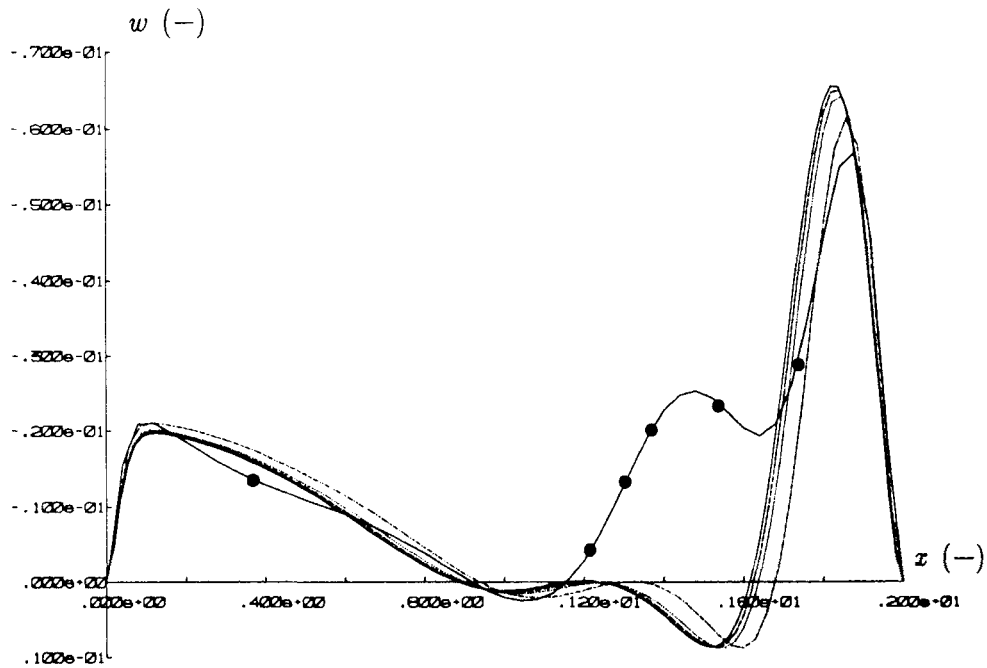

Figure 2. Influence of grid size on axial velocity at symmetry line: ——, 111 × 71; – – –, 101 × 71; ····, 91 × 71; –···–, 71 × 51; —●—, 51 × 51

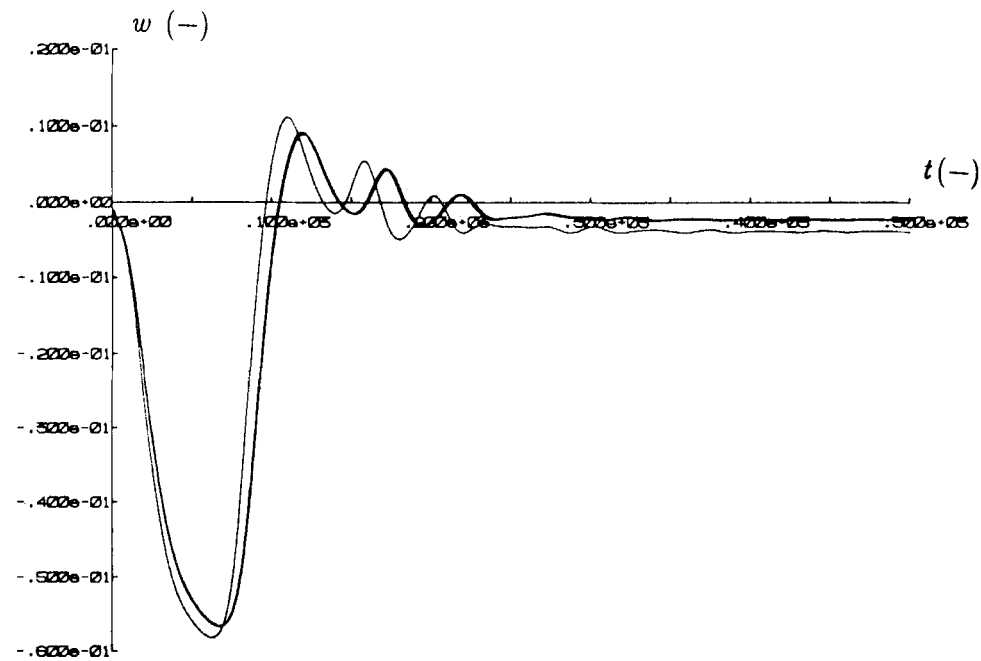

Figure 3. Influence of boundary conditions on axial velocity: ——, second-order, equation (36); – – –, second-order, equation (37); ····, first-order, equation (34)

The time discretization is related to the x-spacing by $\Delta t = C\Delta x$, where the constant C is limited by the CFL condition. Trying different values of C for the present example, it was found that when utilizing second-order accurate boundary conditions, stable solutions could be obtainable for $C \leq 15$, whereas solutions for the first-order accurate conditions were obtained for $C \leq 30$. If higher values of C were employed, the behaviour of the solution history clearly signalled the CFL condition being violated. This is illustrated in Figure 4, where the solution history subject to the boundary condition (37) is shown for C-values 5, 10, 15 and 20. For $C \leq 15$ the solution is almost independent of the time discretization, whereas $C = 20$ results in a clearly unphysical solution history subject to large-amplitude oscillations which quickly grow bigger than the representation of the machine.

Figure 5 shows lines of constant ψ at different times after the start of the cover rotation. It is seen that the fluid motion in the beginning is initiated at the corner $(x, y) = (0, 1)$, from which it penetrates the cylinder. Along the rotating cover is shown the development of an Ekman layer and along the lateral boundary of the cylinder is shown the evolving Stewartson layer.

Following the evolution of fluid motion in time, at $t = 50$ the streamlines are seen to be monotonic, after which an undulating shape slowly appears. At about $t = 100$ a small bubble with recirculating flow appears on the axis of symmetry. This bubble quickly grows and at $t = 110$ it has evolved into two distinct bubbles. In the transient phase these two bubbles are seen to coalesce in a cyclic manner into a coherent mushroom-shaped structure. A steady state is reached at about $t = 350$ where the final structure consists of a large counter-rotating bubble followed immediately downstream by a smaller one.

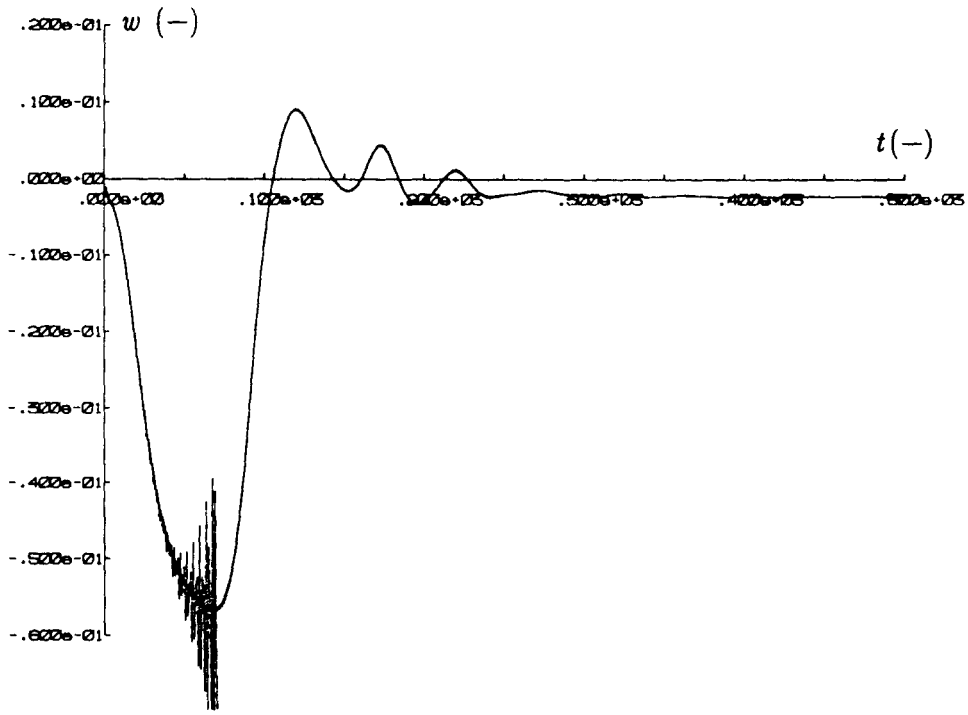

Figure 4. Influence of time step on axial velocity: ——, $C = 5$; – – –, $C = 10$; –·–, $C = 15$; ····, $C = 20$

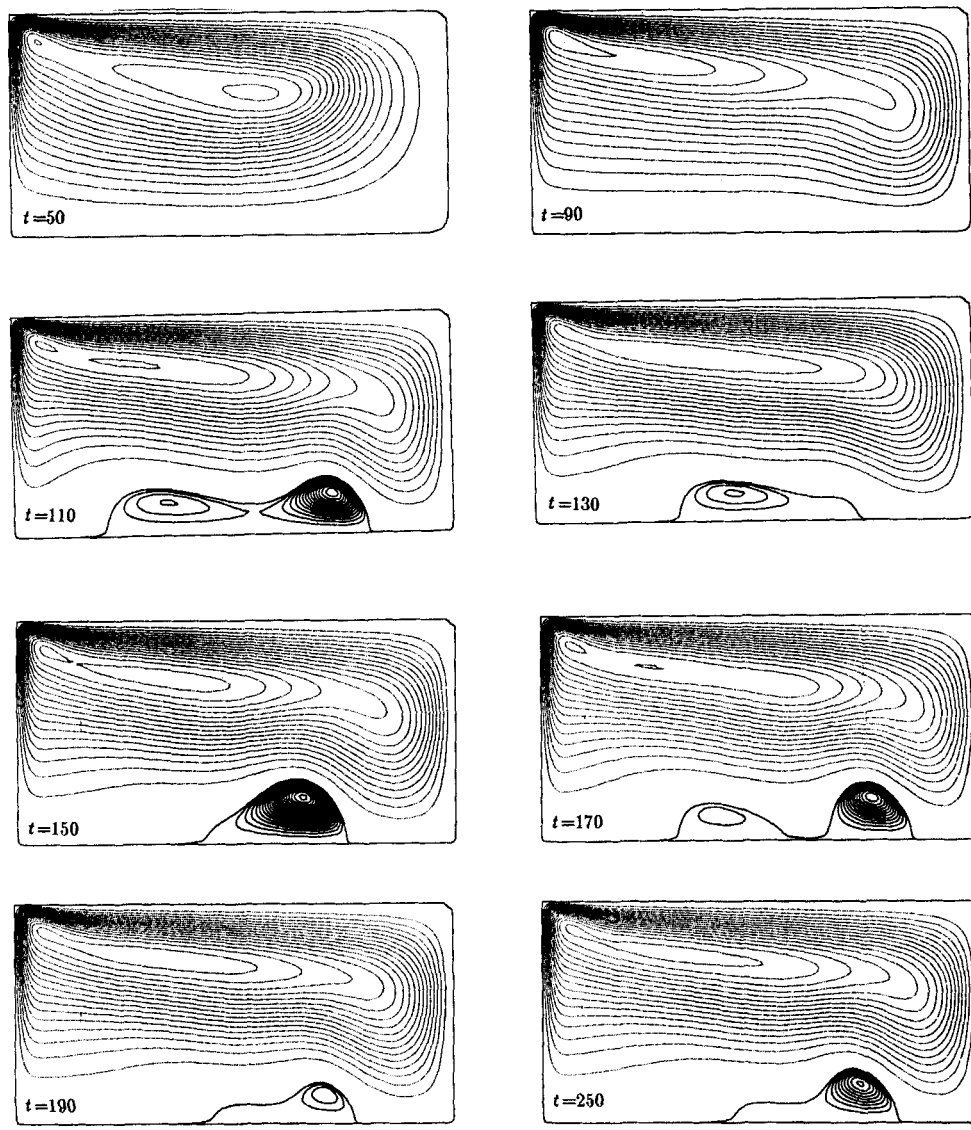

Figure 5. Time series of streamfunction; aspect ratio $H/R = 2{\cdot}0$, $Re = 1854$

The steady state solution is compared in Figure 6 with the visualization of Escudier.[8] In general the visualization and the calculation are in good agreement; however, the onset of the stagnation point of the large bubble differs by an amount of about 3% of the cylinder height.

Another calculation was made for a cylinder with aspect ratio $H/R = 1{\cdot}0$ rotating at a Reynolds number of 1800. This case has been experimentally investigated by Michelsen[9] using an LDA technique to determine velocity distributions. Figures 7 and 8 show tangential and radial velocity distributions respectively along $y = \text{constant}$ lines. In general the calculations are seen to be in excellent agreement with the measurements over most of the flow field; however, owing to the

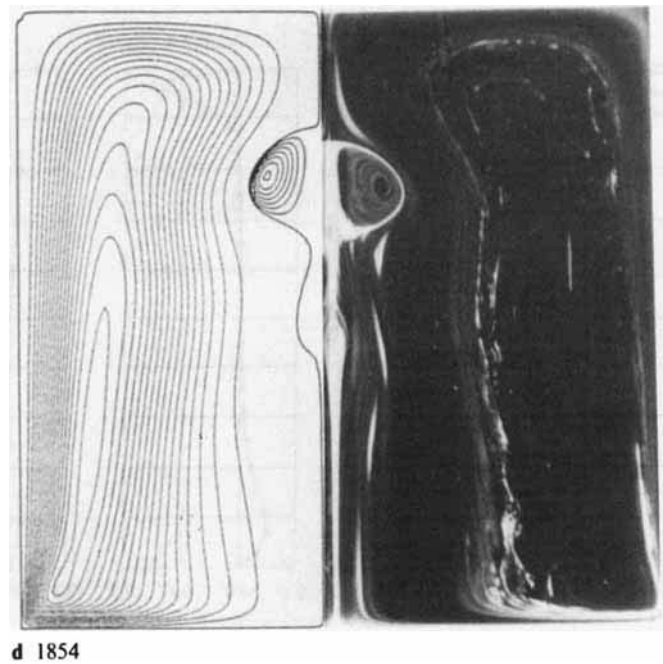

Figure 6. Comparison of calculated streamlines with visualization of Escudier;[8] aspect ratio $H/R = 2{\cdot}0$, $Re = 1854$

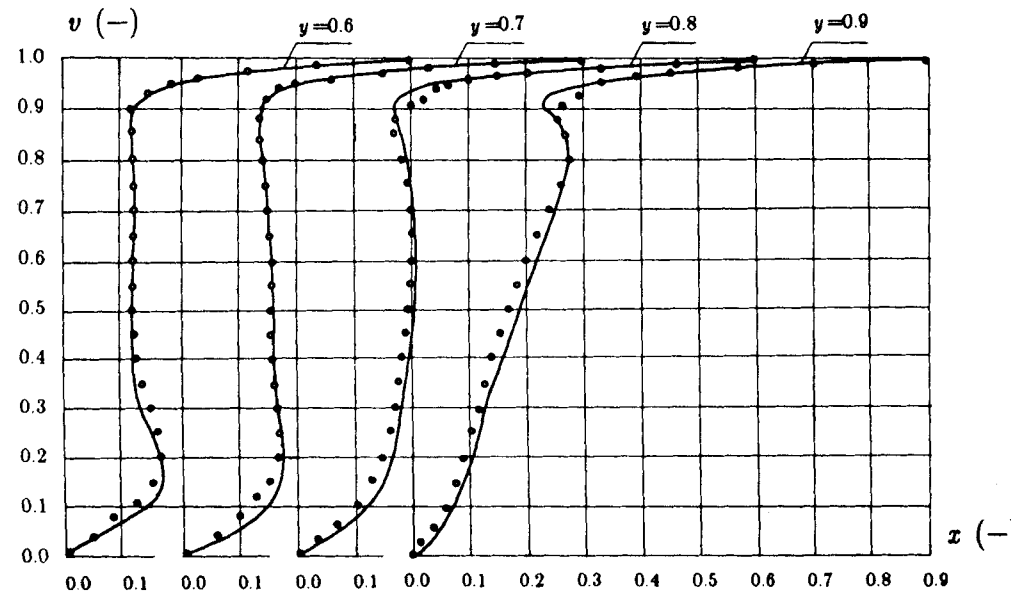

Figure 7. Rotational velocity profiles along y = constant lines: ○, experiments;[9] ——, calculations

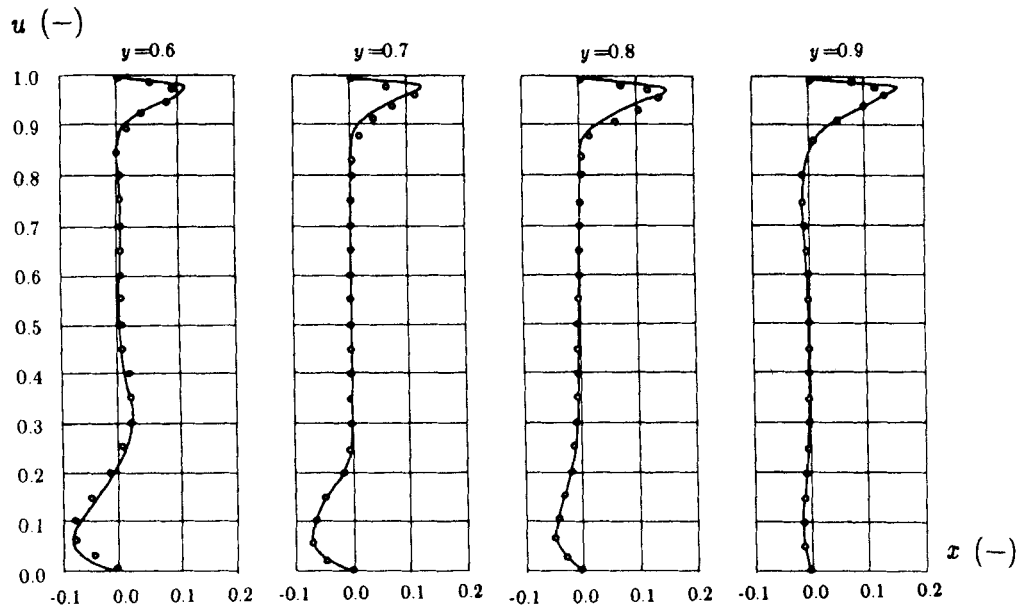

Figure 8. Radial velocity profiles along y = constant lines: ○, experiments;[9] ——, calculations

boundary layer near the boundaries, some deviations may be found. It is reasonable to assume that a finer discretization of the grid near the boundaries will circumvent this deviation.

4.2. Axial flow developing in a stationary pipe

To study the influence of inflow and outflow boundary conditions on a swirl-free flow, we perform a calculation of a flow developing in a pipe with constant cross-section. At the entrance of the pipe the axial velocity distribution is assumed uniform, after which, under the influence of viscous forces, it gradually becomes parabolic. Measurements of this case have been performed by J. Nikuradse and are reproduced by Schlichting.[11]

Introducing the initial axial velocity at the entrance, w_0, as the characteristic velocity and the radius of the pipe, R, as the characteristic length, the Reynolds number is defined as $Re = Rw_0/\nu$ and the inflow conditions are given as

$$x=0: \quad \Gamma=0,\ w=1,\ \psi=-\tfrac{1}{2}y^2. \tag{38}$$

To derive the remaining inflow conditions, we have to make some assumptions which may not necessarily be in accordance with the actual behaviour of the flow. Taking for example $u=0$ implies, owing to the equation of continuity, that $\partial w/\partial x=0$, which puts an unphysical constraint on the incoming flow. A better approximation is obtained by letting the radial velocity be a result of the calculation. This can be done by imposing the Neumann condition $\partial u/\partial x=0$, which corresponds to assuming zero vorticity at the entrance. Since this implies that $\partial\omega/\partial r=0$ all over the inflow plane, an estimate of the error introduced may be derived by evaluation of equation (4) and (8). This results in the condition $\partial^2 w/\partial x^2=0$; thus the introduced error is found to be of second order. In this case the remaining boundary conditions on the entrance are written as

$$\omega=\partial u/\partial x=\partial^2\psi/\partial x^2=0, \tag{39}$$

from which the radial velocity is obtained by performing a Taylor expansion in the flow domain:

$$u_{1,j}=(\psi_{2,j}-\psi_{1,j})/\Delta x r_j+o[(\Delta x)^2]. \tag{40}$$

At a finite distance downstream from the entrance, the velocity distribution becomes fully developed and an outflow condition is defined by putting derivatives with respect to x equal to zero:

$$x=L/R: \quad u=\frac{\partial\psi}{\partial x}=\frac{\partial w}{\partial x}=\frac{\partial\omega}{\partial x}=\Gamma=0, \tag{41}$$

where L denotes the length of the pipe and the Neumann conditions $\partial(\ )/\partial x$ are approximated by the relation $(\ )_{NX,j}-(\ )_{NX-1,j}=0$. After having determined the axial velocity and the vorticity, the second derivative of the streamfunction is updated by employing equation (13), and the streamfunction is determined by employing a third-order Taylor expansion in the x-direction.

At the lateral boundary $y=1$ we employ the same boundary conditions as in the previous test example, i.e. those given by equations (30c), (32) and (36).

According to measurements and approximate analytical studies,[11] the length necessary to make the flow fully developed is uniquely determined by the ratio x/Re. Consequently the flow becomes fully developed only if the channel is sufficiently long or if the Reynolds number is comparatively small.

In the present calculation we put $L=5R$ and $Re=20$, which assures that the flow is fully developed at the outflow boundary.

The influence of the node spacing is examined by trying different values of NX and NY. This is shown in Figure 9, where the axial velocity distribution at the axis of symmetry is compared for

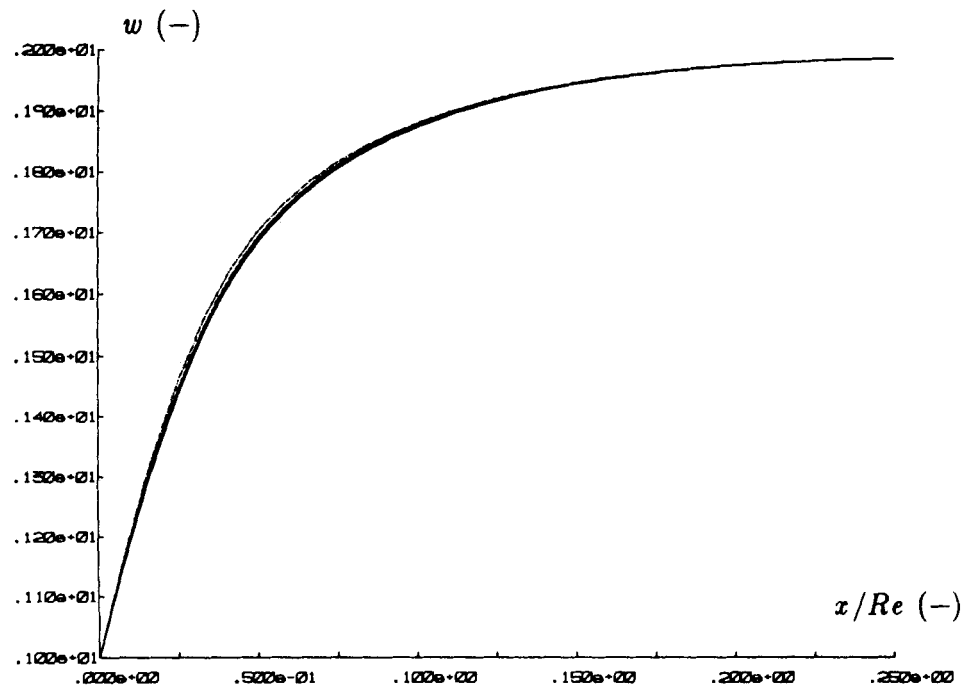

Figure 9. Influence of grid size on axial velocity at symmetry line: –·–, 31 × 21; ····, 31 × 31; – – –, 61 × 31; ——, 61 × 61

$NX \times NY$ values 31×21, 31×31, 61×31 and 61×61. The results show that a node spacing of 31×31 is sufficient to accurately determine the considered velocity distribution.

The sensitivity to the inflow conditions is tested by comparing the second-order accurate conditions defined by equation (39) and (40) with the first-order accurate ones given by assuming $u=0$ all over the inflow plane. In the latter case equation (39) is replaced by letting the vorticity be determined by the Taylor expansion

$$\omega_{1,j}=\left(\frac{\partial^2\psi}{\partial x^2}\right)_{1,j}\Big/ r_j=\frac{2(\psi_{2,j}-\psi_{1,j})}{\Delta x^2 r_j}+o(\Delta x). \tag{42}$$

The outcome of this study is shown in Figure 10, where the resulting distributions of axial velocity along the symmetry line are compared with the measurements of J. Nikuradse (Reference 11, Chap. XI, Figure 11.8). It is seen here that the condition defined by equations (39) and (40) is in much better agreement with the measurements than the one given by equation (42), since the latter immediately downstream of the entrance plane tends to make w constant in a way which does not correspond to the measured behaviour of the flow.

Employing the inflow conditions (39) and (40), a complete comparison between measurements and calculations is shown in Figure 11, where axial velocity distributions at different $y=$constant lines are shown as function of the parameter x/Re. It is seen here that the calculations over most of the pipe are in good agreement with the experimental values. In the immediate neighbourhood of the entrance, however, some discrepancies are seen. These are probably connected with the problem of defining appropriate inflow conditions.

In order to derive some more general outflow conditions, we employ the present configuration to test three different formulations for the boundary condition. Common to them all is that we parabolize the vorticity equation at the outflow. This is accomplished by setting the second x-derivative of the vorticity equal to zero and results in the following expression:

$$\frac{\partial\omega}{\partial t}+\frac{\partial(w\omega)}{\partial x}+f\frac{\partial(u\omega)}{\partial y}=\left[\left(g+\frac{f}{r}\right)\frac{\partial\omega}{\partial y}+f^2\frac{\partial^2\omega}{\partial y^2}-\frac{\omega}{r^2}\right]\Big/ Re. \tag{43}$$

Employing a three-point leap-frog-like discretization in time, we approximate equation (43) by the general formula

$$\begin{aligned}&\frac{\omega^{n+1}_{NX,j}-\omega^{n-1}_{NX,j}}{2\Delta t}+\frac{f_j}{2\Delta y}(u_{NX,j+1}\omega^n_{NX,j+1}-u_{NX,j-1}\omega^n_{NX,j-1})\\&+\frac{1}{\Delta x}\left(w_{NX,j}\frac{\omega^{n+1}_{NX,j}+\omega^{n-1}_{NX,j}}{2}-w_{NX-1,j}\omega^n_{NX-1,j}\right)\\&\quad=\left[\left(g+\frac{f}{r}\right)_j\frac{\omega^n_{NX,j+1}-\omega^n_{NX,j-1}}{2\Delta y}+f_j^2\frac{\omega^n_{NX,j+1}-2\omega^n_{NX,j}+\omega^n_{NX,j-1}}{(\Delta y)^2}-\frac{\omega^n_{NX,j}}{r_j^2}\right]\Big/ Re,\end{aligned} \tag{44}$$

from which the updated vorticity $\omega^{n+1}_{NX,j}$ is derived explicitly.

The first boundary condition is defined by assuming fully developed axial flow:

$$\partial w/\partial x=u=\partial\psi/\partial x=0. \tag{45}$$

Combining equation (45) with equations (8), (11) and (13) and employing second-order accurate approximations, the remaining variables are expressed as follows:

$$w_{NX,j}=w_{NX-1,j}, \tag{46a}$$

$$\left(\frac{\partial^2\psi}{\partial x^2}\right)_{NX,j}=r_j\left(\omega_{NX,j}+f_j\frac{w_{NX,j+1}-w_{NX,j-1}}{2\Delta y}\right), \tag{46b}$$

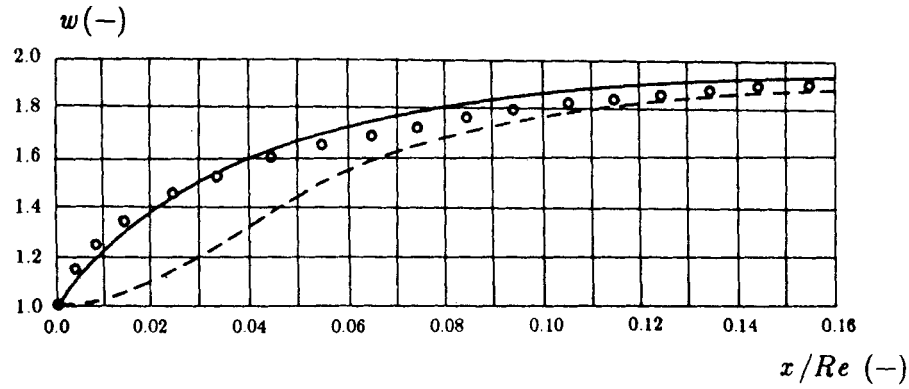

Figure 10. Influence of inflow conditions on axial velocity at symmetry line: ○, measured;[11] ——, $du/dx=0$; – – –, $u=0$

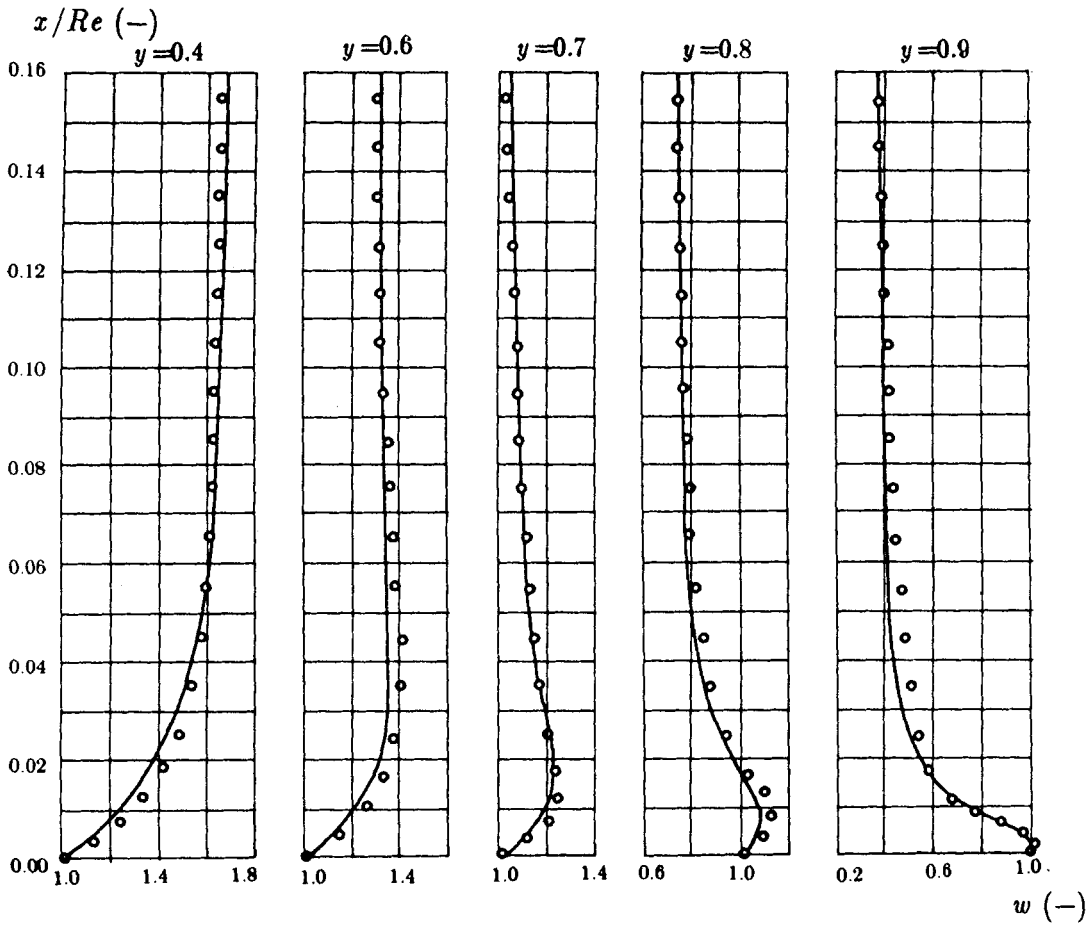

Figure 11. Axial velocity profiles along $y=$constant lines: ○, experiments;[11] ——, calculations

$$\psi_{NX,j}=\psi_{NX-1,j}-\frac{(\Delta x)^2}{2}\left(\frac{\partial^2\psi}{\partial x^2}\right)_{NX,j}. \tag{46c}$$

The other outflow conditions are given by assuming the radial flow be fully developed:

$$\partial u/\partial x=\partial^2\psi/\partial x^2=0. \tag{47}$$

In this case the streamfunction can be obtained either directly from equation (47) by employing a Taylor expansion or from equation (13), which then defines a two-point boundary value problem along the outflow boundary. To see whether the two formulations produce any difference in the results obtained, both will be considered in the following.

The first formulation is obtained directly from a Taylor expansion:

$$\psi_{NX,j}=2\psi_{NX-1,j}-\psi_{NX-2,j}. \tag{48}$$

Employing second-order accurate central differences, the second formulation is given by the solution of equation (13):

$$\left(\frac{f_{j+1}^2}{\Delta y^2}+\frac{(g-f/r)_{j+1}}{\Delta y}\right)\psi_{NX,j+1}-\left(\frac{f_j^2}{(\Delta y)^2}\right)\psi_{NX,j}+\left(\frac{f_{j-1}^2}{(\Delta y)^2}-\frac{(g-f/r)_{j-1}}{\Delta y}\right)\psi_{NX,j-1}=r_j\omega_{NX,j},$$
$$j=2, 3, \ldots, NY-1, \tag{49}$$

subject to the boundary conditions $\psi_{NX,NY}=-1/2$.

For both formulations the velocities are determined from the following discretization formulae:

$$u_{NX,j}=u_{NX-1,j}, \tag{50a}$$

$$w_{NX,j}=-f_j(\psi_{NX,j+1}-\psi_{NX,j-1})/2\Delta y r_j. \tag{50b}$$

To prevent oscillations, we update the outflow variables by averaging between the old values and the newly calculated ones; thus for all the cases considered we update by employing the following relaxation formula:

$$(\,)_{NX,j}^{n+1}=0{\cdot}5\,[(\,)_{NX,j}+(\,)_{NX,j}^{n}]. \tag{51}$$

Now, to summarize, the three outflow conditions to be tested are as follows:

condition A: fully developed axial flow, equations (44) and (46a)–(46c)
condition B: fully developed radial flow, equations (44), (48), (50a) and (50b)
condition C: fully developed radial flow, equations (44), (49), (50a) and (50b)

The test is performed by moving the outflow boundary upstream and evaluating the influence of this on the flow upstream of the new outflow boundary.

In Figure 12 the outflow boundary is imposed at $L=R$ (corresponding to $L=0{\cdot}05Re$) and for the three outflow conditions axial velocity distributions along the co-ordinate lines $y=0$ and $y=0{\cdot}9$ are compared with the original distribution. All three conditions are seen to have an upstream influence corresponding to about half the length of the calculation domain. Furthermore, it is seen that the condition of fully developed radial flow (condition B or C) disturbs the upstream flow less than the assumption of fully developed axial flow (condition A). The difference between the two conditions of fully developed radial outflow is barely seen, but condition C seems to be in better agreement with the original distribution than condition B.

Moving the outflow boundary further upstream to $L=R/2$ makes these tendencies clearer, as shown in Figure 13. Thus evaluating the axial velocity at a point defined by the intersection of the downstream boundary with the axis of symmetry, compared with an original value of 1·45,

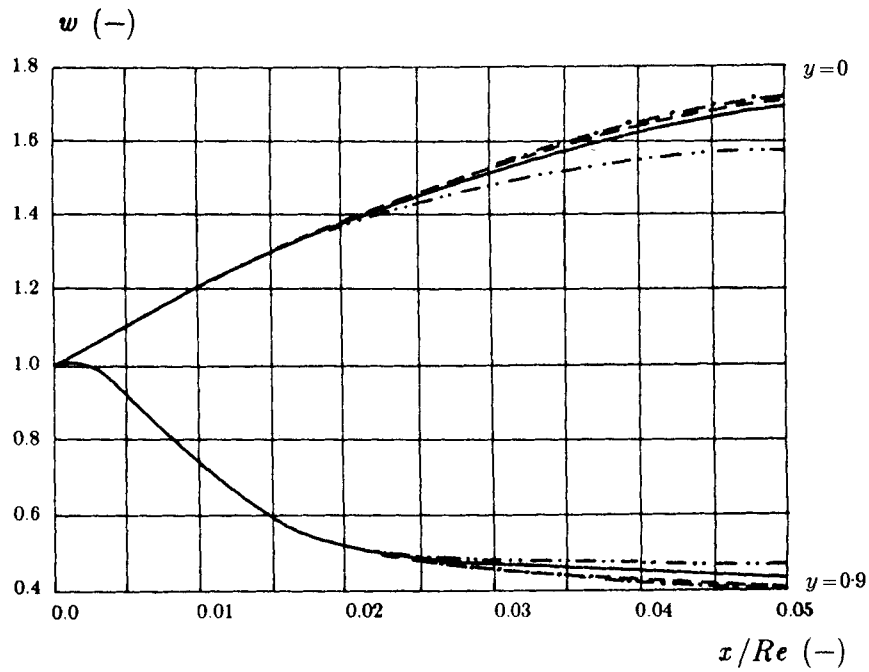

Figure 12. Influence of outflow conditions on axial velocity distributions: ——, undisturbed; –··–, condition A; –·–, condition B; – – –, condition C

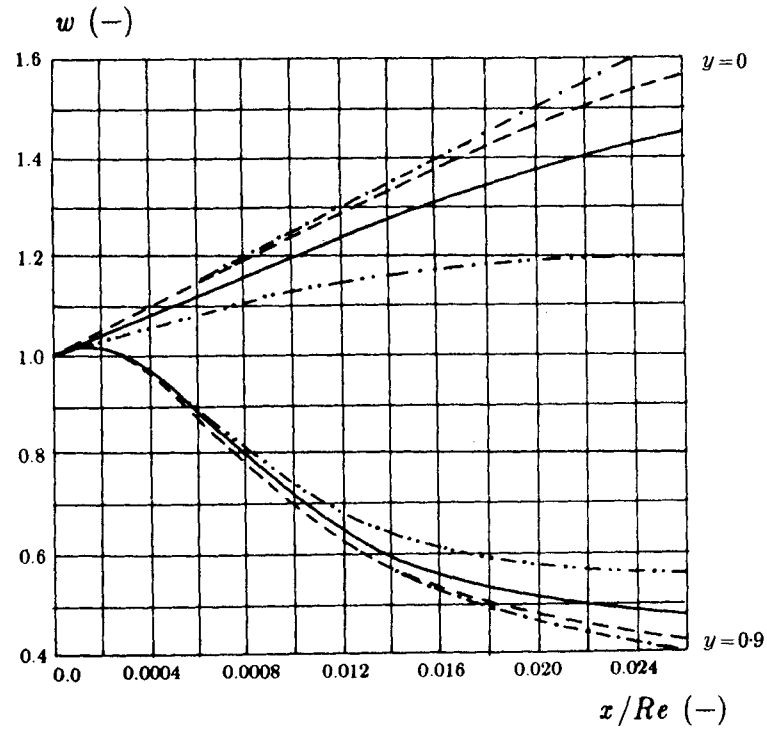

Figure 13. Influence of outflow conditions on axial velocity distributions for axial flow developing in stationary pipe: ——, undisturbed; –··–, condition A; –·–, condition B; – – –, condition C

condition A results in a value of 1·2, condition B predicts a value of 1·65 and condition C gives a value of 1·55.

Comparing the axial velocity distributions in Figure 13, it is seen that all the imposed outflow conditions have an upstream influence which is now perceptible all over the flow domain. It is also seen that the trend manifested near the outflow boundary holds generally in the fluid domain; thus the distributions predicted by condition C are everywhere in better accordance with the undisturbed distributions than those predicted by condition B, which, on the other hand, predicts better results than condition A.

4.3. Developing flow in a rotating pipe

To study the influence of outflow boundary conditions on a rotating flow, we here present some calculations of a flow developing in a rotating pipe. As before, we let the inflow be defined by a uniform axial velocity w_0 and, furthermore, we let the pipe rotate with rotational speed Ω. Assuming fully developed circulation at the outflow boundary, the additional boundary conditions for the circulation are given as follows:

$$x=0: \qquad \Gamma=0, \tag{52a}$$

$$x=L/R: \quad \partial\Gamma/\partial x=0, \tag{52b}$$

$$y=0: \qquad \Gamma=0, \tag{52c}$$

$$y=1: \qquad \Gamma=R\Omega/w_0, \tag{52d}$$

where, as before, all variables have been non-dimensionalized with w_0 and R.

In the present calculation we put $\Omega=w_0/R$ and $Re=100$.

In the case of the non-rotating pipe, it was found that a length of $x/Re=0{\cdot}25$ was sufficient to assure fully developed axial flow. In the present case, trying different pipe lengths, it was found that a value of $x/Re=0{\cdot}5$ was necessary to assure the rotational velocity to be fully developed at outflow. Thus we now limit the calculation domain by $y=1$ and $x=L/R=50$, for which a discretization of 40 points in the y-direction and 500 in the x-direction was employed.

Figure 14 shows tangential velocity distributions at different $y=$constant positions as a function of the axial co-ordinate parameter x/Re. Since the interaction between swirl and axial velocities is essentially non-linear in character, it is not possible to obtain an analytical solution and the authors are not aware of any experiments that may verify the results obtained. However, it is seen that the theoretical tangential velocity distribution $v=y$ is approached when the outflow boundary is reached.

As in the non-rotating case, we again analyse the influence of outflow conditions by moving the outflow boundary upstream. The boundary conditions to be tested are the same as before (conditions A, B and C of the Section 4.2), but they are now combined with the condition of fully developed circulation.

Imposing the outflow conditions at an axial position $L=0{\cdot}005Re$, we compare the calculated tangential velocity distributions with the original distribution. The result of this is shown in Figure 15, where tangential velocity distributions as a function of axial position are shown along the coordinate lines $y=0{\cdot}8$ and $y=0{\cdot}9$.

It is seen here that, in comparison to the non-rotating case, the rotation does not seem to have any appreciable influence on the behaviour of the boundary conditions employed. Thus, although not very different from the distribution of condition B, condition C results in a velocity distribution which is closer to the original one than the other two conditions and it is seen that when moving the boundary conditions upstream the flow is disturbed within a distance which is approximately the same for the three boundary conditions considered.

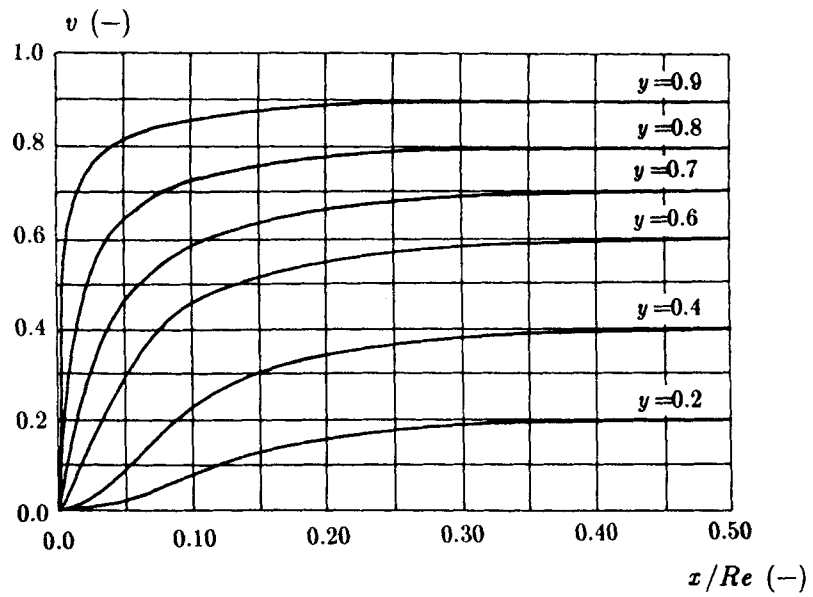

Figure 14. Rotational velocity profiles along y = constant lines for swirl flow developing in rotating pipe

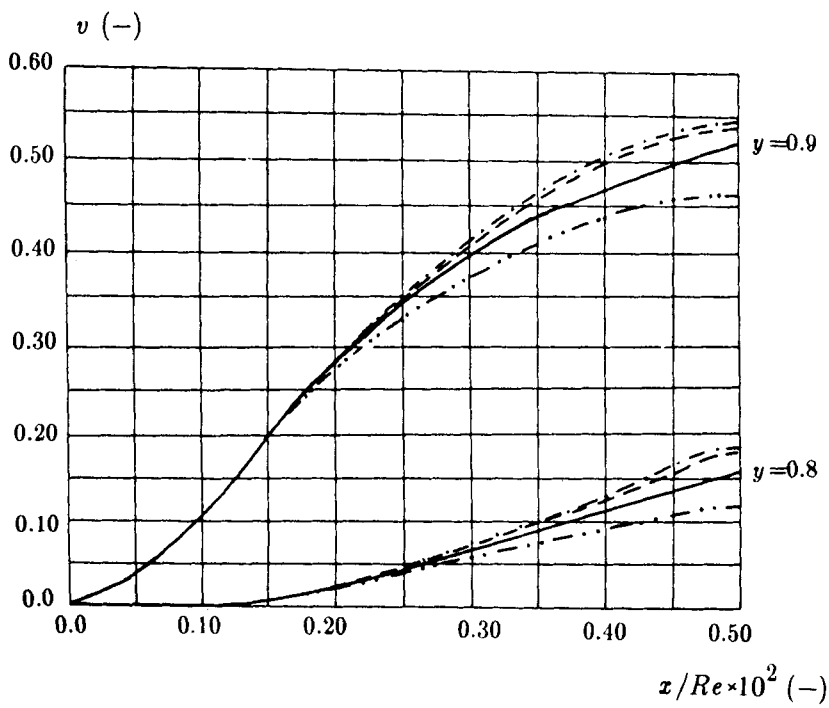

Figure 15. Influence of outflow conditions on axial velocity distributions for flow developing in rotating pipe: ——, undisturbed; –···–, condition A; –·–, condition B; – – –, condition C

5. CONCLUSIONS

In this paper a high-order finite difference solution procedure for the axisymmetric Navier–Stokes equations has been presented.

Comparison of calculated results with experiments confirms the efficiency of the high-order numerical scheme. Thus, for both the flow driven by a rotating cover in a circular container and developing axial flow in a pipe, the presented results are generally in excellent agreement with measured as well as visualized data.

A study of the influence of boundary conditions on solid walls revealed that significant differences may be obtained when comparing results from first-order conditions with results from second-order conditions. Consequently, although the use of first-order conditions results in better stability conditions with faster convergence, it is not recommended to employ conditions of order less than two since the error introduced may be too high.

To study the influence of open flow boundary conditions in axisymmetric configurations, calculations for different inflow and outflow conditions have been performed for developing flow both in a stationary pipe and in a pipe rotating with angular velocity Ω. In disagreement with experimental data, it was found that assuming zero radial velocity, $u=0$, at the inflow boundary forced the axial velocity distribution to be nearly constant and equal to zero just downstream of the inflow section. A much better agreement with experimental results was obtained by replacing this condition with that of $\partial u/\partial x=0$, where u is updated after each iteration.

Three different outflow conditions were tested. Employing in all cases a condition of parabolized vorticity transport, the outflow conditions tested were made by assuming fully developed axial flow, fully developed radial flow with ψ calculated directly from a Taylor expansion and fully developed radial flow with ψ determined from the ψ–ω equation. In the text, these three conditions are referred to as conditions A, B and C respectively. Imposing at first the outflow plane so far downstream that the upstream influence of the outflow conditions was negligible in the first part of the pipe, the influence of the imposed outflow conditions was estimated by letting them move a certain distance upstream and comparing the obtained velocity distributions with the undisturbed ones. From this study the three conditions were found approximately to influence the same distance upstream. However, conditions B and C ($\partial u/\partial x=0$) were everywhere in better agreement with the undisturbed distributions than condition A ($u=0$).

ACKNOWLEDGEMENTS

This work was done when one of the authors (J.N.S.), sponsored by the Danish Technical Research Council, was on leave at Division OAt2 at ONERA, Châtillon. The authors would like to express their appreciation to Drs. C. Teissedre, T. K. Dang and Y. Morchoisne for their kind hospitality during the stay and for many valuable discussions during the course of this investigation.

REFERENCES

1. Ta Phuoc Loc and O. Daube, 'Unsteady viscous flow around a circular cylinder at moderate Reynolds numbers', *Numerical Methods for Laminar and Turbulent Flows*, Pineridge Press, Swansea, 1985, pp. 631–642.
2. Ta Phuoc Loc and A. Bouard, 'Numerical solution of the early stage of the unsteady viscous flow around a circular cylinder: a comparison with experimental visualization and measurements', *J. Fluid Mech.*, **160**, 93–117 (1985).
3. L. Mane and Ta Phuoc Loc, 'Simulation d'ecoulements instationnaires a grands nombres de Reynolds sur une architecture parallel', *La Recherche Aerospatiale*, No. 2, 49–58 (1987).
4. O. Daube, Ta Phuoc Loc, P. Monnet and M. Coutanceau, 'Ecoulement instationnaire decolle d'un fluide incompressible autour d'un profil, une comparison theorie-experience', *AGARD Conf Proc. No.* 386, 1985, pp. 3.1–3.14.
5. L. Collatz, *The Numerical Treatment of Differential Equations*, Springer-Verlag, New York, 1986.

6. R. S. Hirsh, 'Higher order accurate difference solutions of fluid mechanics problems by a compact differencing technique, *J. Comput. Phys.*, **19,** 90–109 (1975).
7. E. L. Wachpress, *Iterative Solutions of Elliptic Systems*, Prentice-Hall, Englewood Cliffs, NJ, 1966.
8. M. P. Escudier, 'Observations of the flow produced in a cylindrical container by a rotating endwall, *Exp. Fluids*, **2,** 189 (1984).
9. J. A. Michelsen, '*Modeling of laminar incompressible rotating fluid flow*', *AFM 86-05, Ph.D. Dissertation*, Department of Fluid Mechanics, Technical University of Denmark, 1986.
10. H. Lugt and M. Abboud, 'Axisymmetric vortex breakdown with and without temperature effects in a container with a rotating lid, *J. Fluid Mech.*, **179,** 179–200 (1987).
11. H. Schlichting, *Boundary-Layer Theory*, McGraw-Hill Series in Mechanical Engineering, New York, 1968.